# Death of period-doublings: locating the homoclinic-doubling cascade

Bart E. Oldeman [1], Bernd Krauskopf [2] and Alan R. Champneys [3]

*Department of Engineering Mathematics, University of Bristol, Bristol BS8 1TR, UK*
*Applied Nonlinear Mathematics Research Report 99.19, November 1999*

**Abstract**

This paper studies a natural mechanism, called a homoclinic-doubling cascade, for the disappearance of period-doubling cascades in vector fields. Simply put, an entire period-doubling cascade collides with a saddle-type equilibrium. Homoclinic doubling cascades are known to have self-similar structure. In contrast to the well-known Feigenbaum constant, the scaling constants for homoclinic-doubling depend on the eigenvalues of the saddle equilibrium.

Specifically, we present here for the first time a detailed study of homoclinic-doubling cascades in a smooth vector field, namely a three-dimensional polynomial model proposed by Sandstede. A numerical algorithm is presented for computing homoclinic-doubling cascades in general vector fields, which makes use of the program AUTO/HOMCONT. This allows us to compute two types of homoclinic-doubling cascades, one where the primary homoclinic orbit undergoes an inclination flip bifurcation and one where it undergoes an orbit flip bifurcation. Our results bring out the scaling constants in good agreement with analytical estimates obtained from one-dimensional maps.

*Key words:* period-doubling cascades; bifurcations; homoclinic-doubling; numerical continuation.
*PACS:* 02.30.Hq; 02.40.Vh; 02.60.Lj; 05.45.+b

## 1 Introduction

Period-doubling is a central phenomenon within dynamical systems with many applications and well-developed theory; see for example [1] and references therein.

[1] E-mail: Bart.Oldeman@bristol.ac.uk, tel: +44-117-9289798, fax: +44-117-9251154, corresponding author
[2] E-mail: B.Krauskopf@bristol.ac.uk
[3] E-mail: A.R.Champneys@bristol.ac.uk

Feigenbaum [2] explored the well-known universality of sequences or *cascades* of successive period doublings and derived the corresponding accumulation rate or *scaling constant* of the appropriate renormalisation operator. This constant is equal to $4.699\ldots$ and is now called the Feigenbaum constant. Period-doubling cascades require a single parameter to be varied, but as one varies a second parameter, they can be created or destroyed. One possibility is that a forward period-doubling cascade is followed by a reverse cascade as a single parameter is varied. In the parameter plane this corresponds to islands of nested period-doubling curves. See for example [3] for a particular mechanism likely to cause this, and [4] for peiord-doubling islands in a laser system.

This paper concerns a different possibility of destroying a period-doubling cascade. The primary periodic orbit at the head of this cascade collides with a saddle equilibrium with real eigenvalues to form a homoclinic orbit. The same then happens to each subsequent orbit in the period-doubling cascade, resulting in the death of the cascade in its entirety. As a second parameter is changed, the period of each $2^n$-periodic limit cycle approaches infinity and in the limit a *homoclinic-doubling cascade* is obtained. This was first studied numerically in [5] for a piecewise-linear vector field and then proved to exist in generic families of vector fields in [6]. Figures 1 and 2 below illustrate this process. All the periodic orbits involved in the period-doubling cascade in Figure 1 collide with the saddle in Figure 2. In the process $n$-homoclinic orbits are created for $n = 2^i, i = 0\ldots5$, that is, orbits that start in the unstable manifold of the saddle point and come close to this same equilibrium a further $n-1$ times before returning to the saddle point as $t \to \infty$. A system in which such a phenomenon exists must have at least two parameters, one controlling the period-doubling bifurcations and one controlling the period of the orbits. In parameter space, this corresponds to a sequence of period-doubling bifurcation curves, all ending in codimension-two bifurcations involving homoclinic orbits. What this bifurcation looks like is explained in Section 2, and it is sketched in Figure 6. Going from left to right in the lower half of this figure results in a periodic-doubling cascade, whereas doing the same in the top half one finds no period-doublings at all. At so called *homoclinic-doubling bifurcations* $\mathbf{B_n}$ a $2n$-homoclinic orbit is spawned from an $n$-homoclinic orbit, giving also rise to a period-doubling and a saddle-node bifurcation curve. Note that the accumulation rate of the points $\mathbf{B}$ is not the same as the usual Feigenbaum number of the period doublings. In fact there are two scaling constants and these depend on the eigenvalues of the saddle points as is explained in Section 4 below; see also [5,7].

Homoclinic-doubling can be caused by codimension-two bifurcations involving a change in the orientation of the vector field around the homoclinic orbit: so called *orbit flips* and *inclination flips*. These are defined carefully in Section 2 below. They are specific to the case where all eigenvalues of the equilibrium are real. In the case of complex eigenvalues $n$-homoclinic orbits are much more common [8], but these do not concern us here. Orbit flip homoclinic orbits, which are non-principal, were mainly treated by Sandstede [9]. Inclination flip or critically twisted

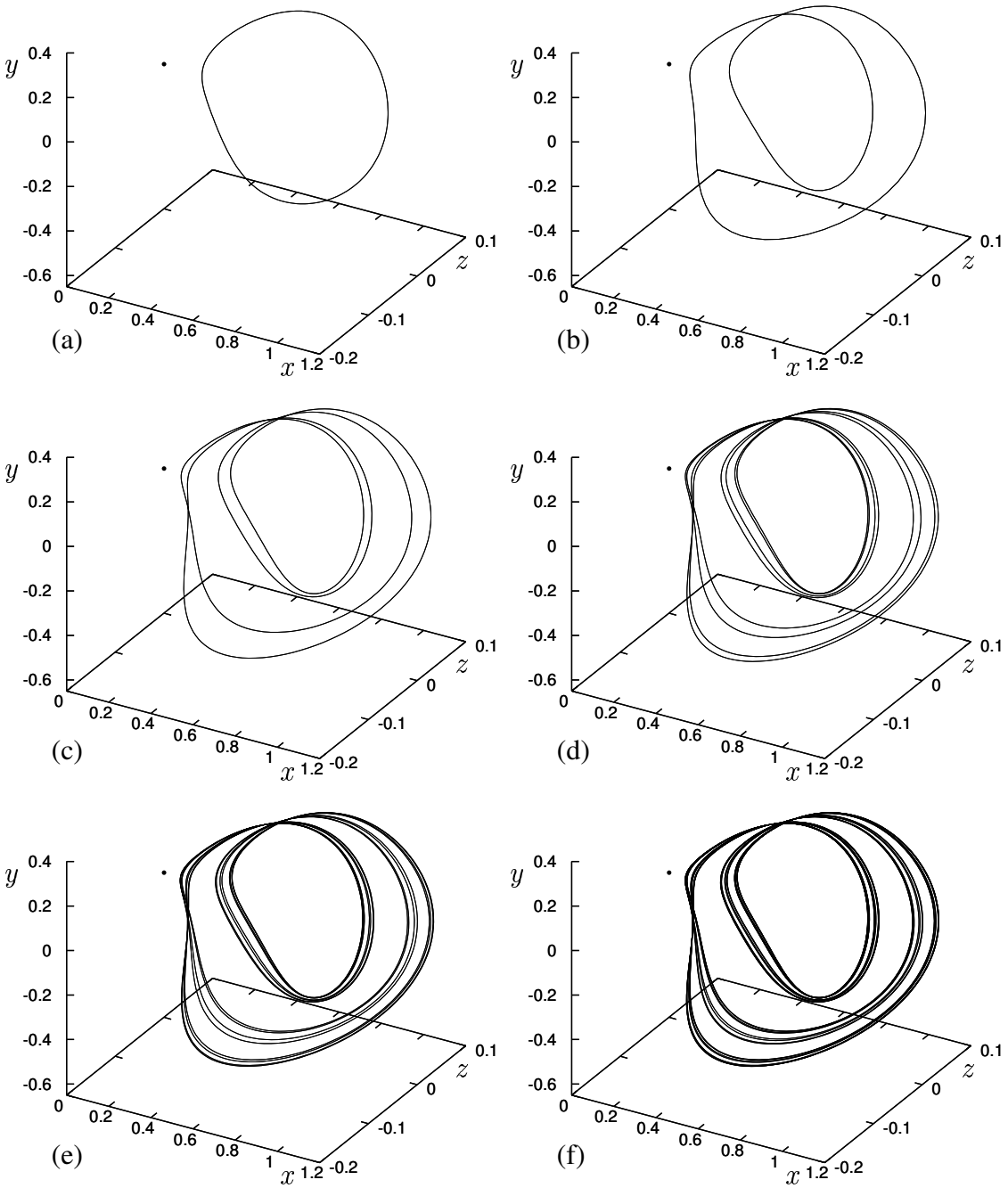


Fig. 1. Periodic orbits in phase space of a period-doubling cascade. The panels show $n$-periodic orbits where $n$ runs in powers of two from 1 to 32 from (a) to (f). The results are for Sandstede's model (1) with parameter values given in the first row of Table 2 and $\mu = -0.02$. The values of $\alpha$ are $1.109084, 1.091685, 1.088392, 1.087699, 1.087551$ and $1.087519$, respectively.

homoclinic orbits have been investigated by Homburg, Kokubu and Naudot [6], Kisaka, Kokubu and Oka [10,11] and Naudot [12]. For certain configurations of eigenvalues at the saddle point these homoclinic flip bifurcations cannot only cause homoclinic-doubling, but may also generate chaos; see Section 2 for more details.

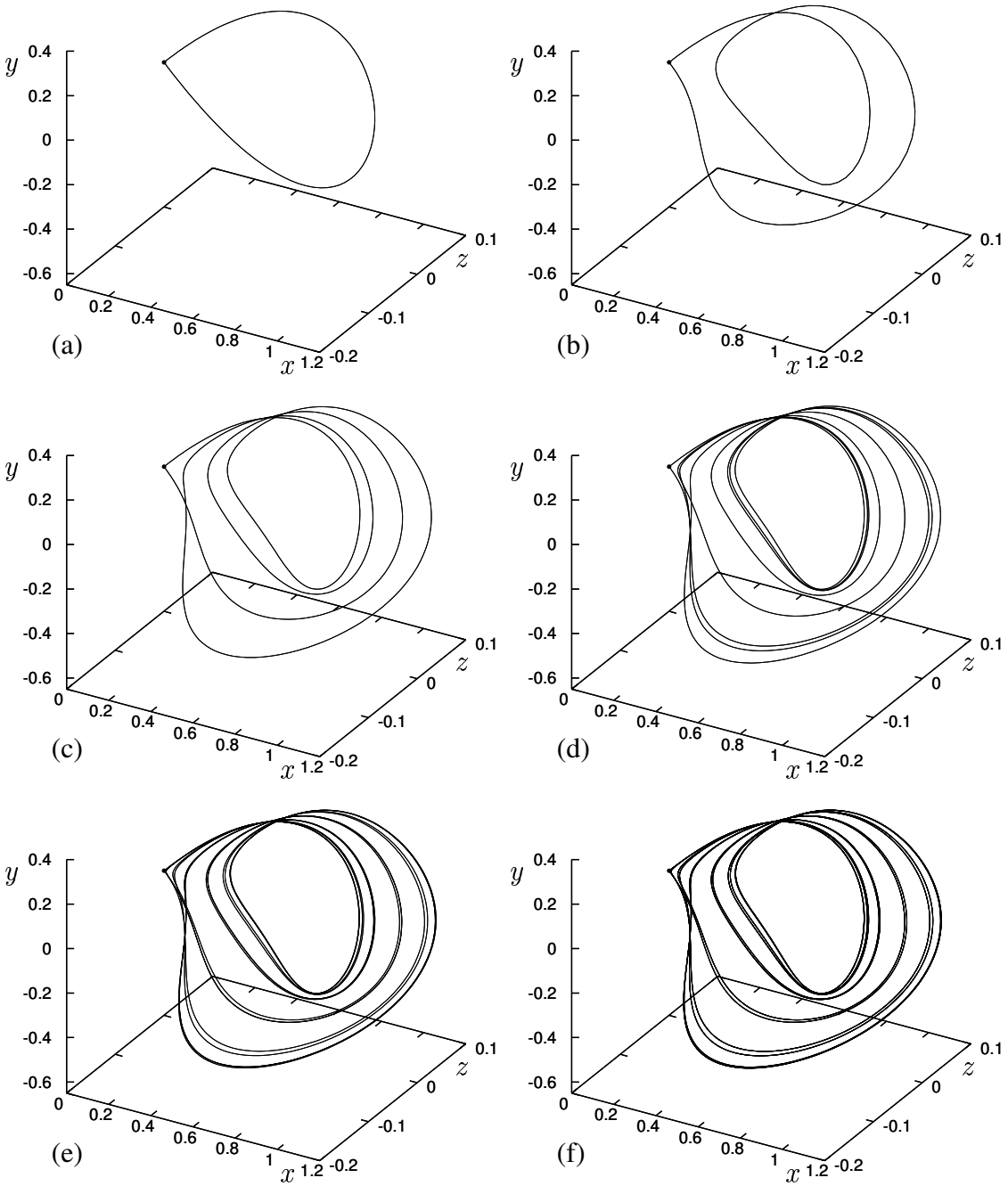


Fig. 2. Homoclinic orbits in phase space of a homoclinic-doubling cascade. The panels show $n$-homoclinic orbits where $n$ runs in powers of two from 1 to 32 from (a) to (f). Notice how each homoclinic orbit corresponds to a periodic orbit from Figure 1 having hit the saddle point at the origin. The results are for model (1) with parameter values in the top row of Table 2, where $(\alpha, \mu)$ are $(1.121, 0)$, $(1.109084, -8.975602 \cdot 10^{-3})$, $(1.091685, -1.364093 \cdot 10^{-2})$, $(1.088392, -1.435636 \cdot 10^{-2})$, $(1.087699, -1.445927 \cdot 10^{-2})$ and $(1.087551, -1.448071 \cdot 10^{-2})$, respectively.

Different applications in which homoclinic flip bifurcations occur have also been studied. Amongst these are the FitzHugh-Nagumo nerve-axon equations [13], Koper's

model for electro-chemical oscillators [14], and the Shimitzu-Morioka equations for convection instabilities [15–17]. In each of these applications a single inclination flip was found, but no specific investigation was made to see if it is part of a larger homoclinic-doubling cascade. Many other examples of applications of homoclinic bifurcations and homoclinic chaos can be found in [18].

A purpose of this paper is to present a numerical algorithm to *find* a homoclinic-doubling cascade, that is, to numerically locate the successive homoclinic-doubling points and all bifurcation curves involved. Our investigations confirm the theory in [6,19] about the existence of a homoclinic-doubling cascade and closely correspond to the results of [5] where a piecewise-linear vector field and a one-dimensional map modelling a general homoclinic-doubling cascade are considered. The novel approach in this paper is that a smooth vector field is used, which can be seen as typical, so that it serves as a model for what homoclinic-doubling cascades look like in applications. The specific model we take is that introduced by Sandstede [20], which was specifically constructed to admit the global bifurcations under consideration here. The numerics are performed with AUTO/HOMCONT [15,21,22].

The paper is organized as follows. In Section 2 we give an overview of the theory on the codimension-one and -two bifurcations that are relevant to the homoclinic-doubling cascade treated in here. Section 3 then introduces Sandstede's model and presents the results of our numerical investigations. Homoclinic-doubling cascades triggered by an inclination flip and by an orbit flip are treated in detail. In the process we describe a general numerical procedure for computing homoclinic-doubling cascades in example systems. In Section 4 the scaling laws of the homoclinic-doubling cascade from our numerical results are examined and compared with iterates of appropriately defined one-dimensional maps. A good agreement is found between our numerical results and the existing theory. Section 5 contains conclusions, a general discussion and an outlook to future research.

## 2 Homoclinic bifurcations

In this section we review results from the homoclinic bifurcation theory literature that are relevant for our study of the death of a period-doubling cascade in a homoclinic-doubling cascade. We first consider codimension-one homoclinic orbits to a saddle point with real eigenvalues. The homoclinic doublings occur at codimension-two homoclinic flip bifurcations which we explain before reviewing what is known about the homoclinic-doubling cascade itself. We explain that homoclinic-doubling cascades can be found near certain codimension-three homoclinic bifurcations called resonant homoclinic flip points.

To be more precise, consider bifurcations of a homoclinic orbit to a hyperbolic equilibrium in a three-dimensional vector field. Note that, by homoclinic center

manifold techniques, these results are also valid in higher dimensional spaces; see [23,24]. The equilibrium can be taken to be the origin and is assumed to have two stable (negative) and one unstable (positive) eigenvalue, denoted by $-\lambda_{ss}$, $-\lambda_s$ and $\lambda_u = 1$, respectively. Note that it is always possible to scale any vector field having a real saddle equilibrium to achieve these eigenvalues (with a reversal of the direction of time if necessary). We further assume that $-\lambda_{ss} < -\lambda_s < 0$.

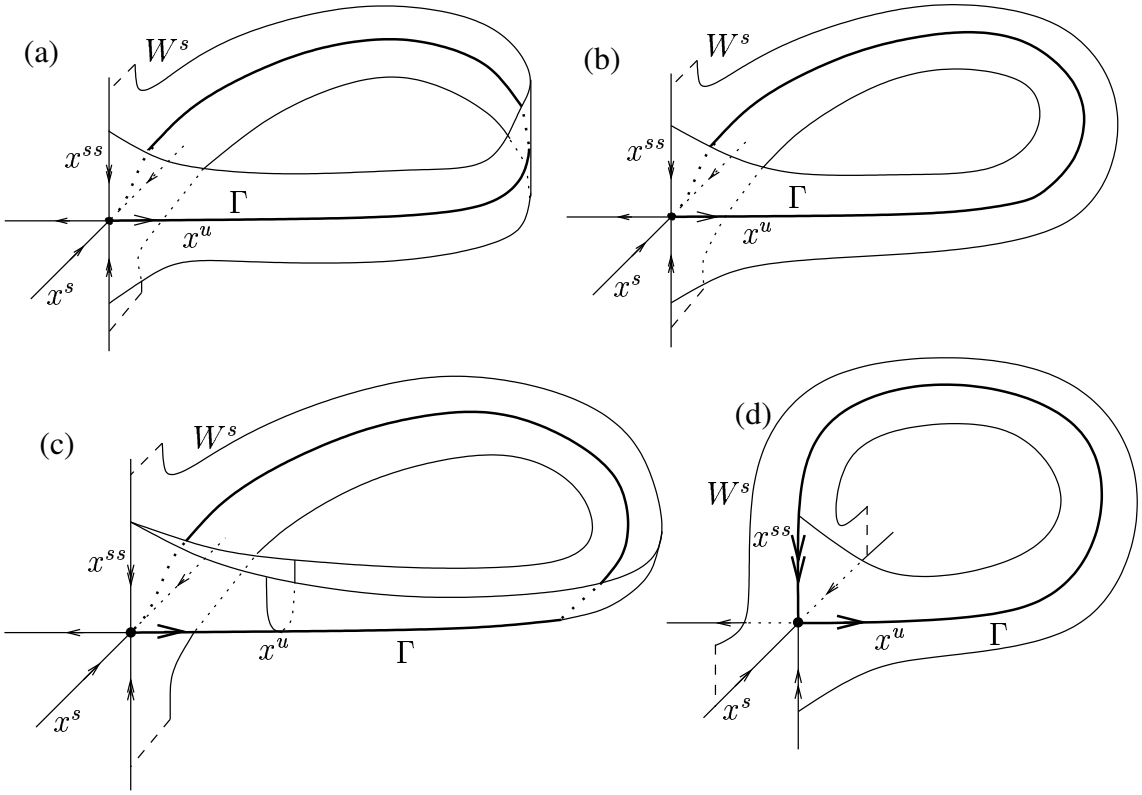


Fig. 3. An orientable (a) and a twisted (b) codimension-one homoclinic orbit. In an inclination flip (c) the orientation of $W^s$ changes. The inclination flip depicted corresponds to the case $\lambda_{ss} > 2\lambda_s$, investigated here. If $\lambda_{ss} < 2\lambda_s$, the stable manifold is shallow instead of sharp at the unstable direction near the equilibrium. The orientation of $W^s$ also changes in an orbit flip (d).

A homoclinic orbit to such a saddle point, such as those in Figure 2, is generically of codimension-one. The genericity conditions that need to be satisfied (see also [19] for more discussion) are

(G1) $\lambda_s \neq 1$

(G2) In positive time the homoclinic orbit approaches the origin tangent to the weak stable direction, which is the eigenvector associated with $-\lambda_s$.

(G3) The two-dimensional stable manifold $W^s$ returns tangent to the strong stable direction, if followed backwards in time along the homoclinic orbit. This is called the strong inclination property [25,26].

A key observation is that for a generic codimension-one homoclinic orbit there are two geometrically different possibilities. The stable manifold $W^s$ when followed along the homoclinic orbit is either orientable or twisted. This is depicted in Figure 3 (a) and (b), respectively. In the orientable case the stable manifold is topologically a cylinder and in the twisted case it is a Möbius strip. This distinction turns out to be crucial in what follows.

If exactly one of the above genericity conditions fails then there is a codimension-two bifurcation. Violation of (G1) gives a *resonant homoclinic orbit* [27]. This case does not occur in the homoclinic-doubling cascade we investigate in this paper. If either (G2) or (G3) fails one speaks of a *homoclinic flip bifurcation*, namely of an *orbit flip* if (G2) is not satisfied and of an *inclination flip* if (G3) is not satisfied. The homoclinic orbit at a homoclinic flip bifurcation is depicted in Figure 3(c) for the inclination flip and in Figure 3(d) for the orbit flip.

For both an orbit flip and an inclination flip the stable manifold is neither orientable nor twisted, but is somewhere "in between"; see Figure 3 (c) and (d). Passing through either of these bifurcations changes the orientation of the stable manifold $W^s$, hence the name homoclinic *flip* bifurcation. It turns out that the dynamics in a neighbourhood (in parameter and phase space) of an orbit flip and an inclination flip behave essentially in the same way. The key feature of these flips is that the stable manifold changes its orientation; see also [28].

For a homoclinic flip bifurcation to be of codimension two extra genericity conditions must be satisfied. This leads to three cases. Which case occurs depends on the eigenvalues $\lambda_s$ and $\lambda_{ss}$ as depicted in Figure 4. Note that, although the bifurcations in these cases are qualitatively the same for both the orbit flip and the inclination flip, the eigenvalue conditions defining the case are different.

| Notation | Description |
|---|---|
| $n^s$ | A *stable* $n$-periodic orbit exits. |
| $n^u$ | An *unstable* $n$-periodic orbit of saddle type exits. |
| $SN^n$ | A saddle-node bifurcation of $n$-periodic orbits. |
| $PD^n$ | A period-doubling of an $n$-periodic orbit. |
| Hopf | A Hopf bifurcation. |
| $H^n_{t/o}$ | A twisted ($t$) or orientable ($o$) $n$-homoclinic bifurcation. |
| • | All codimension-two bifurcations (such as homoclinic flips, cusp, degenerate Hopf, degenerate $PD$) are marked by a dot. |

Table 1
The notation used in the bifurcation diagrams

**A** No extra bifurcations occur.

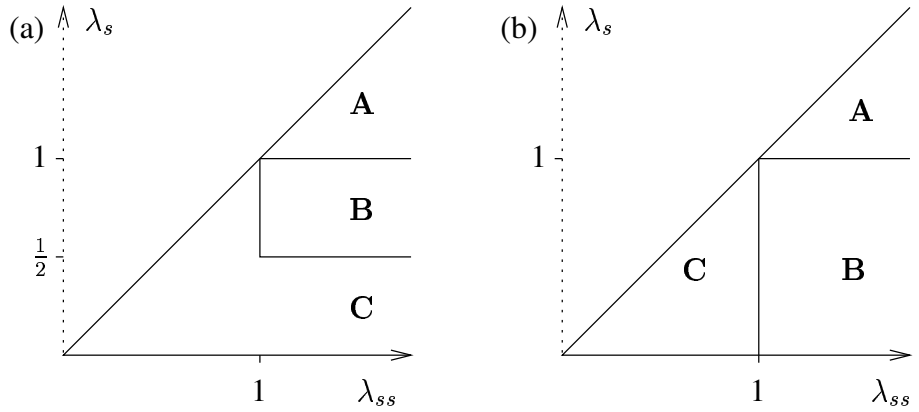


Fig. 4. Eigenvalue regions in which the codimension-two unfolding of an inclination flip (a) and an orbit flip (b) are of the types **A**, **B** and **C** sketched in Figure 5.

**B** A *homoclinic-doubling bifurcation* occurs. This involves a period-doubling bifurcation $PD^1$ and a 2-homoclinic bifurcation $H_o^2$ on the twisted side and a saddle-node bifurcation $SN^1$ on the orientable side.

**C** The bifurcation diagram consists of a fan of infinitely many $n$-periodic and $n$-homoclinic orbits for arbitrary $n$ and a region with horseshoe dynamics.

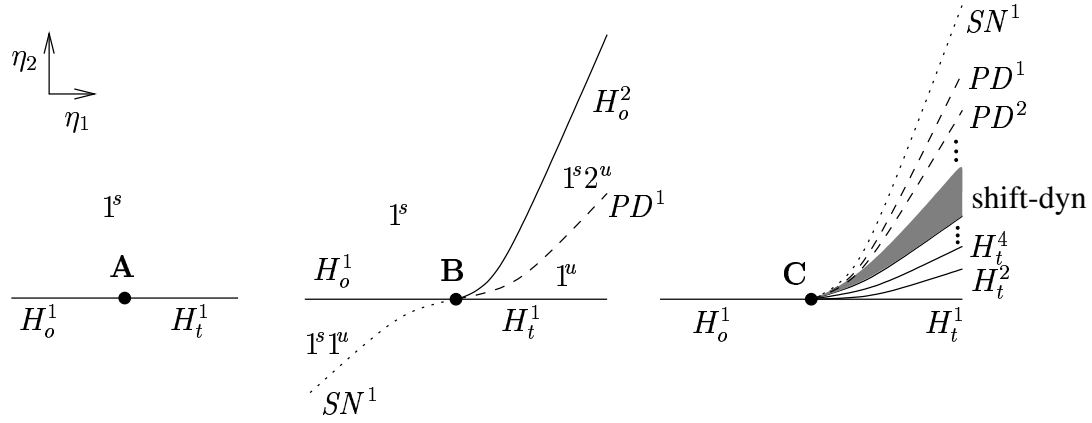


Fig. 5. The different cases of codimension-two homoclinic flip bifurcations for the eigenvalue conditions in Figure 4. In **A** there are no extra bifurcations, **B** is called homoclinic-doubling, and **C** depicts one configuration of an infinite bifurcation fan involving the creation of chaotic dynamics through the break-up of a horseshoe.

Bifurcation diagrams of the associated unfoldings are given in Figure 5, where $\eta_1$ breaks the flip and $\eta_2$ breaks the existence of the homoclinic orbit. The structure of the unfolding of a bifurcation of type **B** was found in [10,11,6] for the inclination flip, and in [9] for the orbit flip. For an overview of the fan depicted in Figure 5 and the other possibilities for type **C** see [19] and further references therein. The main tool in the literature for analysing homoclinic-doubling cascades is the use of one-dimensional unimodal maps, which are reductions of Poincaré mappings along the homoclinic orbit. These maps may also be derived in a functional analytic fashion using a method due to X.B. Lin; see [9]. The one-dimensional maps are especially useful for investigating the scaling laws, as is discussed in Section 4.

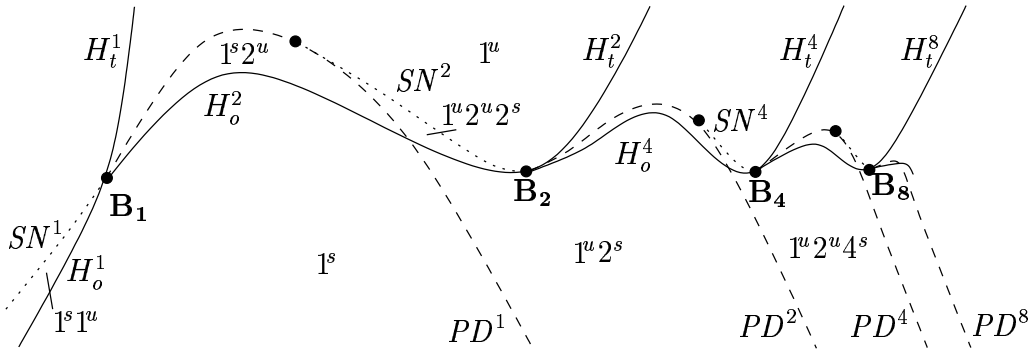


Fig. 6. Qualitative sketch of a homoclinic-doubling cascade. Orientable homoclinic orbits undergo homoclinic-doubling in the points $\mathbf{B_{2^n}}$, which accumulate at a limit. Cutting across this structure from left to right below the cascade results in a period-doubling cascade. The saddle-node bifurcations make the structure consistent.

The codimension-two homoclinic flip bifurcations of type $\mathbf{B}$ in Figure 5(b) are the main building blocks of a homoclinic-doubling cascade, and we now discuss them in detail. In this and subsequent diagrams we use the notation given in Table 1. Not only are the bifurcation curves labelled, but also the limit cycles in different regions of the bifurcation diagram are denoted as being either stable or unstable by the use of the superscripts $s$ or $u$. This is of great help for checking that the bifurcation diagrams are consistent. The primary homoclinic orbit changes from orientable to twisted at the homoclinic flip bifurcation point $\mathbf{B}$, changing the curve $H_o^1$ to $H_t^1$. A saddle node curve $SN^1$ originates at $\mathbf{B}$ from the orientable side, that is, tangent to $H_o^1$. A period-doubling bifurcation $PD^1$ and an orientable 2-homoclinic bifurcation $H_o^2$ originate at $\mathbf{B}$ on the twisted side, that is, tangent to $H_t^1$. These curves are exponentially close to the homoclinic bifurcation curve $H_{o/t}^1$.

Figure 5(b) is a consistent unfolding as can be checked by making one loop around $\mathbf{B}$ and considering the types of periodic orbits existing in the different regions. As we start counter-clockwise from the lower right-hand corner, where no periodic orbits exist, crossing $H_t^1$ an unstable 1-periodic orbit $1^u$ bifurcates and then undergoes a period-doubling at $PD^1$. Therefore, both a stable 1-periodic orbit $1^s$ and an unstable 2-periodic orbit $2^u$ exist above $PD^1$. The period of $2^u$ then increases and it disappears in $H_o^2$. The periodic orbit $1^s$ continues to exist, even as $H_o^1$ is crossed and an unstable limit cycle $1^u$ bifurcates from $H_o^1$. The periodic orbits $1^s$ and $1^u$ can then be followed until they disappear in the saddle-node curve $SN^1$. Now no limit cycles are present anymore and we are back where we started.

In [6] it was proved for the orbit flip and in [19] for the inclination flip that a homoclinic-doubling cascade occurs near a central codimension-three point on the border between $\mathbf{B}$ and $\mathbf{C}$. That is, there are sequences of $\mathbf{B}$-type homoclinic flips so that $H_o^1$ doubles to $H_o^2$, followed by $H_o^2$ doubling to $H_o^4$, $H_o^4$ to $H_o^8$, and so on. Such a codimension-three point is called a *resonant homoclinic flip bifurcation*. The results can be summarized in the following theorem, which should be read in conjunction with Figure 4.

**Theorem 1** *[6,19] A homoclinic-doubling cascade occurs near one of the following resonant homoclinic flip bifurcations:*

*(a) A primary inclination flip bifurcation on the border from* $\mathbf{B}$ *to* $\mathbf{C}$*, that is for the eigenvalue conditions:*

$$\lambda_{ss} = 1 \qquad \textit{where} \qquad \frac{1}{2} < \lambda_s < 1, \qquad \textit{and}$$
$$\lambda_s = \frac{1}{2} > 0 \qquad \textit{where} \qquad \lambda_{ss} > 1.$$

*(b) A primary orbit flip bifurcation on the border from* $\mathbf{B}$ *to* $\mathbf{C}$*, but only for the eigenvalue conditions*

$$\lambda_{ss} = 1 \qquad \textit{where} \qquad \frac{1}{2} < \lambda_s < 1.$$

*In both cases the cascade consists of inclination flips. It can be found in the region where inclination flips of type* $\mathbf{B}$ *occur, which explains the condition* $\lambda_s > 1/2$ *in (b).*

An intuitive explanation for the fact that all non-primary homoclinic flip bifurcations are inclination flips is that a sequence of inclination flips seems to be more generic than a sequence of orbit flips, as it only involves a qualitative change in the structure of the stable manifold, and not in the structure of the homoclinic orbit itself.

Theorem 1 proves that homoclinic-doubling cascades exist. But, *how* might $\mathbf{B}$-type codimension-two homoclinic flip bifurcations be connected to each other to form a cascade? The simplest consistent way seems to be the one depicted in Figure 6. This was conjectured in [6] and indicated by the numerics on a piecewise-linear vector field in [5]. As we take a closer look, the homoclinic orbit at the curve $H_o^2$ which originates from the flip at $\mathbf{B_1}$ undergoes a further homoclinic flip bifurcation itself. This means that the 2-homoclinic orbit becomes twisted in another homoclinic-doubling bifurcation at $\mathbf{B_2}$. A 4-homoclinic orbit originates from this bifurcation and undergoes a homoclinic flip bifurcation, and so on. From each of the points $\mathbf{B_n}$, a period-doubling bifurcation originates, resulting in a period-doubling cascade where the curves $PD^n$ cross the curves $H_o^{2n}$. This is possible because a degenerate period-doubling bifurcation occurs, so that the period-doubling takes place in the opposite direction and for the opposite stability of the orbits than before. The periodic orbit $(2^{2n})^s$ now disappears, together with an unstable limit cycle $(2^{2n})^u$, at the saddle-node curve $SN^{2n}$ originating from the degenerate period-doubling bifurcation. Now this saddle-node curve can be nicely connected to the next point $\mathbf{B}$ of the corresponding order. The purpose of our numerical investigations in the forthcoming section is to confirm this structure.

The study of the codimension-three singularities at the heart of the parameter in

Theorem 1 is the subject of [29]. We remark that it is relatively straightforward to find a codimension-three resonant homoclinic flip bifurcation numerically using AUTO/HOMCONT. On the other hand, finding an actual homoclinic-doubling cascade is a challenge and as we are about to see it involves many continuation steps.

## 3 Numerical investigation

In this section we investigate the homoclinic-doubling cascade numerically in Sandstede's model, which is introduced in Section 3.1. In Section 3.2 we present a numerical approach that can be used to find homoclinic-doubling cascades in arbitrary vector fields. Sections 3.3 and 3.4 then contain the specific application of this approach to Sandstede's model. We first consider a homoclinic-doubling cascade where the primary homoclinic orbit undergoes a $\mathbf{B}$-type *inclination flip* and second a homoclinic-doubling cascade where it undergoes a $\mathbf{B}$-type *orbit flip*.

### *3.1 Sandstede's model*

The numerical results which follow are all for a model introduced by Sandstede [20]. It was explicitly constructed to contain codimension-two inclination and orbit flips for any eigenvalue configuration. The model is polynomial and is given by the following set of equations:

$$\begin{aligned}
\dot{x} &= ax + by - ax^2 + (\tilde{\mu} - \alpha z)x(2 - 3x) + \delta z, \\
\dot{y} &= bx + ay - \frac{3}{2}bx^2 - \frac{3}{2}axy - (\tilde{\mu} - \alpha z)2y - \delta z, \\
\dot{z} &= cz + \mu x + \gamma xz + \alpha\beta(x^2(1 - x) - y^2).
\end{aligned} \tag{1}$$

Here $a, b, c, \mu, \tilde{\mu}, \alpha, \beta, \gamma$ and $\delta$ are parameters which take particular values at the different bifurcations. In the present context, the parameter $\delta$ may be set to zero.

The vector field was constructed as a perturbation of a vector field in which the Cartesian leaf $\{(x, y, z) | x^2(1 - x) - y^2 = 0, z = 0\}$ is a solution for $(\mu, \tilde{\mu}) = 0$. If we also set $a = 0$ and $b = 1$ then there exists an explicit homoclinic solution to the origin given by

$$(x(t), y(t), z(t)) = (1 - (\frac{1 - e^t}{1 + e^t})^2, 4e^t \frac{1 - e^t}{(1 + e^t)^3}, 0), \tag{2}$$

which is contained in the Cartesian leaf defined here. Using this solution as a starting point, curves of homoclinic orbits can be followed using HOMCONT [22]; see Section 3.2 for details.

The eigenvalues of the linearisation at the origin are given by

$$\lambda_{1,2} = a \pm \sqrt{b^2 + 4\tilde{\mu}^2}, \quad \lambda_3 = c.$$

In this setting we take $|a| < b, 0 < b$ and $c < 0$ and the eigenvalues are fixed at $-2$, $-0.75$ and $1$. We use the following properties of (1).

**Theorem 2** *[20] A homoclinic solution* $\Gamma$ *of* (1) *contained in the Cartesian leaf,* $\{(x, y, z)|x^2(1 - x) - y^2 = 0, z = 0\}$ *exists for* $(\mu, \tilde{\mu}) = 0$. *Furthermore, the following holds:*

*(a) An inclination flip occurs for* $c < a - b$ *and* $\beta = 1$. *This bifurcation is unfolded by the parameters* $\mu$ *and* $\alpha - \alpha_0$ *for a certain* $\alpha_0$ *depending on* $a, b, c$ *and* $\gamma$. *Moreover, in the unfolding the parameter* $\mu$ *breaks the homoclinic orbit and* $\alpha - \alpha_0$ *changes the orientation of* $W^s$.

*(b) An orbit flip occurs for* $c > a - b$, $\beta = 0$ *and sufficiently small* $\alpha$, *where* $\alpha > 0$. *The unfolding parameters are* $\mu$ *and* $\tilde{\mu}$. *These are both involved in breaking the homoclinic orbit and in changing the orientation of* $W^s$.

This result shows that Sandstede's model is well-suited to study homoclinic-doubling cascades, both where the primary homoclinic bifurcation is an inclination flip and where it is an orbit flip. By exhaustive numerical computations we have found these homoclinic-doubling cascades in this model. We first give the algorithm we used to obtain such a cascade, and then present our results for both types of homoclinic flip bifurcations in detail.

### *3.2 The general approach*

For our numerical investigation we used the package AUTO [22], which includes the homoclinic continuation code HOMCONT. AUTO is a general two-point boundary value code, employing Gauss–Legendre collocation and pseudo-arclength continuation. AUTO can continue periodic orbits as one parameter varies. It can also detect and continue period-doubling and saddle-node bifurcations of periodic orbits. In AUTO, the period of any periodic orbit is rescaled to one and solution data is represented at a defined number $\texttt{NTST} \times \texttt{NCOL}$ of points, where `NTST` is the number of mesh intervals and `NCOL` (typically $\texttt{NCOL} = 4$) denotes the number of so called Gauss collocation points per mesh interval. The coordinates of the orbit are given as mesh points for values of the rescaled time $t$, where $0 \leq t \leq 1$. In the extension HOMCONT a homoclinic orbit is described in the same way, with the additional property that the points at $t = 0$ and $t = 1$ are close to the equilibrium along the stable and unstable linear eigenspaces, respectively. In this setup both periodic orbits and homoclinic orbits can be continued by solving boundary value problems. HOMCONT can also detect orbit flips, and by solving an extended problem using additional information about the orientation of the stable manifold, inclina-

tion flips; see [21]. This latter step involves the solution of the adjoint variational equations, which doubles the size of the system being solved. Both homoclinic flip bifurcations can be continued in three parameters.

The first step in computing homoclinic bifurcations is to find an initial homoclinic orbit. This can be done in HOMCONT by continuing directly from an explicitly given homoclinic solution, by continuing a periodic orbit to infinite period or by homotopy; see [22]. In our subsequent computations we start from the explicit solution (2).

An important ingredient of our method is the ability to switch the continuation from a homoclinic orbit to a periodic orbit and back. AUTO readily switches from a homoclinic orbit to the continuation of the bifurcating high-periodic orbit. However, switching from a high-periodic orbit to a homoclinic bifurcation is more difficult. As the period of the orbit increases, the equilibrium is generally approached for a value of $t$ which is not equal to $0$ or $1$ in the data-structure describing the orbit. Therefore, this structure needs to be rotated in such a way that it starts and ends near the equilibrium. A phase-shift routine that does this is a new feature that we have incorporated into HOMCONT.

If we combine all these capabilities, we can construct an algorithm to find a homoclinic-doubling cascade. One step of this algorithm is as follows:

- Follow a primary $n$-homoclinic orbit as two parameters vary using HOMCONT and detect a homoclinic flip bifurcation, which is either an inclination flip or an orbit flip.
- At some distance along the homoclinic curve from this homoclinic flip bifurcation, switch to the continuation of a periodic orbit using regular AUTO continuation.
- AUTO can detect a period-doubling or a saddle-node bifurcation.
- These bifurcations can then be followed in two parameters.
- At a period-doubling bifurcation, let AUTO switch to the period-doubled orbit and continue it to such a high period that it becomes a good approximation of a homoclinic orbit.
- After using the newly implemented phase-shift routine, this orbit can be continued as a $2n$-homoclinic orbit using HOMCONT.

This process can be repeated arbitrarily many times in theory, but is in practice restricted to $n \leq 32$ in this study due to memory constraints in AUTO/HOMCONT and the increasing numerical accuracy which is needed to continue the bifurcations. Specifically, at each period-doubling the number of mesh points (collocation intervals) `NTST` must be doubled. Starting the algorithm with $\texttt{NTST} = 30$, we found that $n = 32$ was the limit we were able to reach on a moderate sized workstation. Also, at this level, as we see below, certain saddle-node bifurcation curves were found to be too close to other bifurcation curves to be continued in AUTO.

The above algorithm gives a way of calculating a homoclinic-doubling cascade which, once started from the primary homoclinic orbit, only involves continuation. The whole homoclinic-doubling cascade is computed step by step thereafter, and as such, the process could be automated.

### *3.3 Results on the inclination flip*

The above algorithm was applied to obtain a homoclinic-doubling cascade starting with an inclination flip bifurcation of the primary homoclinic orbit. First the different parameters in Sandstede's model need to be fixed. Following Theorem 2(a) we set $\tilde{\mu} = 0$. This simplifies the eigenvalues to $\lambda_1 = a - b$, $\lambda_2 = a + b$ and $\lambda_3 = c$. As stated in Section 3.1, we choose to achieve the eigenvalues $\lambda_1 = -2$, $\lambda_2 = -0.75$ and $\lambda_3 = 1$ and, therefore, set $a = 0.125$, $b = 0.875$ and $c = -2$. These eigenvalues are sufficiently close to the transition between $\mathbf{B}$ and $\mathbf{C}$ mentioned in Theorem 1(a), but far enough to obtain good separation of bifurcation curves. The inclination flip is unfolded by $\alpha - \alpha_0$ for a certain value of $\alpha_0$. As stated in Theorem 2, a homoclinic bifurcation existing at $\mu = 0$ is unfolded by the parameter $\mu$. The parameter $\gamma$ controls a normal-form coefficient in the codimension-two bifurcation in such a way that the curves in the unfolding move closer together or further apart as $\gamma$ is varied. We set $\gamma = 3$. A suitable choice of $\alpha_0$ can be found numerically by continuing a homoclinic orbit in HOMCONT in $\alpha$ and $\mu$. On increasing $\alpha$ from zero, the first inclination flip we found was at $\alpha_0 \approx 1.193035$, and this is the point $\mathbf{B_1}$ from which we started the numerical investigation of the homoclinic-doubling cascade. Table 2 gives an overview of the different parameter values.

| Parameter | $a$ | $b$ | $c$ | $\alpha$ | $\beta$ | $\gamma$ | $\delta$ | $\mu$ | $\tilde{\mu}$ |
|---|---|---|---|---|---|---|---|---|---|
| Inclination flip | $0.125$ | $0.875$ | $-2$ | free | $1$ | $3$ | $0$ | free | $0$ |
| Orbit flip | $-0.5$ | $\sqrt{2.25 - 4\tilde{\mu}^2}$ | $-0.75$ | $1$ | $0$ | $1$ | $0$ | free | free |

Table 2
Parameter values of (1) used in our numerical investigations.

The results of the numerical computations can be found in Figures 7 and 8. The notation is summarized in Table 1, as was also explained in Section 2. This figure consists of homoclinic, period-doubling and saddle-node bifurcation curves, organised by homoclinic inclination flip points $\mathbf{B_n}$ of increasing order into a homoclinic-doubling cascade. The structure of the homoclinic-doubling cascade is brought out further in Figure 8, where the successive panels (a), (b) and (c) are plotted relative to the 1, 2 and 4-homoclinic bifurcation curves $H^1_{o/t}$, $H^2_{o/t}$ and $H^4_{o/t}$, respectively. This means that the vertical axis in each of these panels shows the distance in $\mu$ from the respective homoclinic curve. By applying this technique we obtain a much clearer way of viewing the details than by simply zooming in on the relevant regions in Figure 7. This cascade in Figures 7 and 8 has indeed the structure sketched in Figure 6, but it actually shows what a homoclinic-doubling cascade looks like in a real vec-

tor field. Figures 7 and 8 make the point that one can regard a homoclinic-doubling cascade as the limit of a period-doubling cascade as the period of its orbits goes to infinity. See Figures 1 and 2 for the orbits involved in these two cascades.

Let us explain a few details of how we obtained these results. Starting from the Cartesian leaf solution (2), the primary homoclinic orbit was followed in $\alpha$ and $\mu$, which indeed yielded the horizontal line: $\{\mu = 0\}$ for the bifurcations $H^1_{o/t}$ depicted in Figure 7. At $\alpha = 1.135$, the homoclinic orbit was then used as a starting point for the continuation in the negative $\mu$-direction of an unstable limit cycle $1^u$. AUTO detected a period-doubling bifurcation for $\mu \approx -3.787590 \times 10^{-3}$. This period-doubling bifurcation was continued in two parameters and gives the curve $PD^1$. After that we switched onto the unstable period-doubled limit cycle $2^u$ and continued it in $\mu$. In so doing, the period grows to infinity, a clear sign that the trajectory is becoming a 2-homoclinic orbit. At this point we followed this orbit as a 2-homoclinic orbit, after applying the phase-shift routine mention in Section 3.2. The 2-homoclinic bifurcation was then continued in the two parameters $\alpha$ and $\mu$ to obtain the homoclinic bifurcation curve $H^2_o$. HOMCONT then detected an inclination flip ($\mathbf{B_2}$ at $\mu = 1.121224, \alpha = -6.530211 \cdot 10^{-3}$) for this orbit. From a point with lower $\mu$ on the curve $PD^1$, AUTO detected a new period-doubling bifurcation when the period-doubled orbit $2^u$ was continued for decreasing $\alpha$. Thus we have obtained the periodic orbit $4^u$, which was continued to a 4-homoclinic orbit, and so on. The saddle-node curves were detected and continued by following a periodic orbit from a homoclinic curve or a period-doubling bifurcation. AUTO detected saddle-node bifurcations, which were then continued in two parameters. The saddle-node curves $SN^2$ and $SN^4$ are close to the other neighbouring bifurcation curves. With the curve $SN^8$ this is even more extreme, and the numerical accuracy of AUTO (double precision) is not sufficient to follow it.

Notice the striking self-similarity in Figure 8. The only visual differences between Figures 8 (a), (b) and (c) are the scale and the order of the bifurcations occurring in them. This self-similarity is discussed further in Section 4.

### *3.4 Results on the orbit flip*

We now apply the algorithm in Section 3.2 to find a homoclinic-doubling cascade where the primary homoclinic orbit undergoes an orbit flip. All subsequent homoclinic flips ($\mathbf{B_2}$ and higher) are inclination flips just like in the previous section; see also Theorem 1. In fact, the results for this case are strikingly similar to the previous one, suggesting that the structure of homoclinic-doubling cascades is largely insensitive to whether these flips were brought about by an an orbit flip or an inclination flip. This is another confirmation of the fact that the important ingredient is the flip, that is, the change of orientation of $W^s$; see [28] and [19].

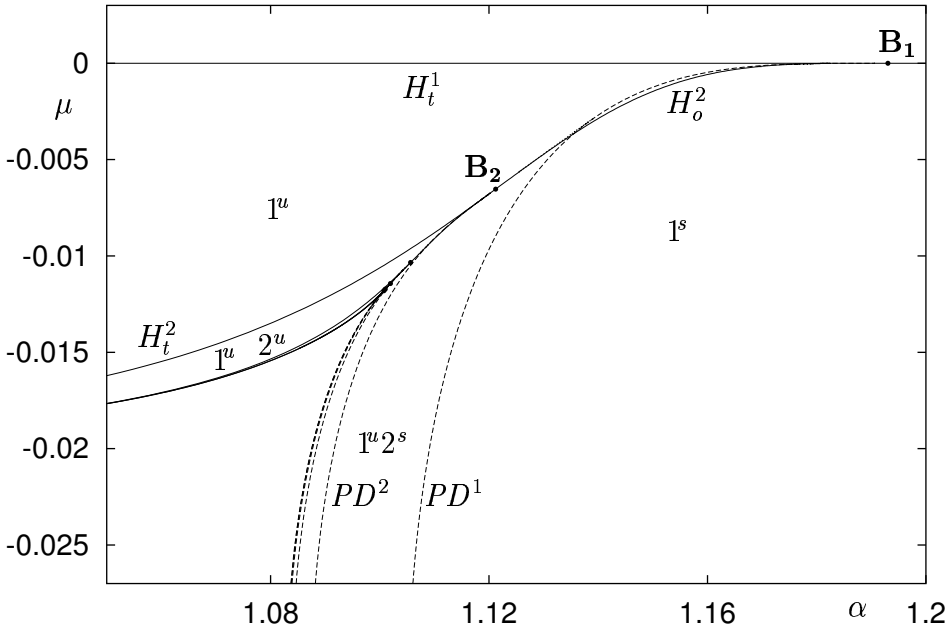


Fig. 7. A numerical picture of a homoclinic-doubling cascade in (1), where the primary homoclinic orbit undergoes an inclination flip at $\mathbf{B_1}$. See the first row of Table 2 for the values of the other parameters.

According to Theorem 2(b), in order to obtain an orbit flip we must have $\alpha$ not too large, $a - b < c$ and $\beta = 0$. Then the homoclinic orbit $\Gamma$ of (1) undergoes a generic orbit-flip bifurcation with respect to the parameters $(\mu, \tilde{\mu})$. Since again we choose to have $\lambda_u = 1$, $\lambda_{ss} = 2$ and $\lambda_s = 0.75$, and $a - b < c$ if $\tilde{\mu} = 0$, we must have that $a$ and $b$ satisfy

$$\begin{aligned} \lambda_{ss} &= -(a - \sqrt{b^2 + 4\tilde{\mu}^2}) = 2, \\ \lambda_u &= a + \sqrt{b^2 + 4\tilde{\mu}^2} = 1, \\ \lambda_s &= -c = 0.75. \end{aligned}$$

These values of eigenvalues are again sufficiently close to the transition $\mathbf{B - C}$ mentioned in Theorem 1(b). Furthermore, we have set $\alpha = 1$ and $\gamma = 1$. See Table 2 for a list of the different parameter values that we used.

For this orbit flip case, the results of the numerical computations can be found in Figures 9 and 10, where the latter shows the consecutive enlargements relative to the curves $H^1_{o/t}$, $H^2_{o/t}$ and $H^4_{o/t}$, just like in Figure 8. These figures consist of the same bifurcation curves as for the inclination flip case, now organised by the orbit flip $\mathbf{B_1}$ and the inclination flips $\mathbf{B_n}$ for $n \geq 2$.

Figures 9 and 10 were computed by starting from the orbit flip at $(\mu, \tilde{\mu}) = (0, 0)$ and continuing the 1-homoclinic curve $H^1_{o/t}$ with HOMCONT. At the point $(0.08, 0.09658088)$, we switched from the homoclinic orbit to the bifurcating periodic orbit $1^u$ for in-

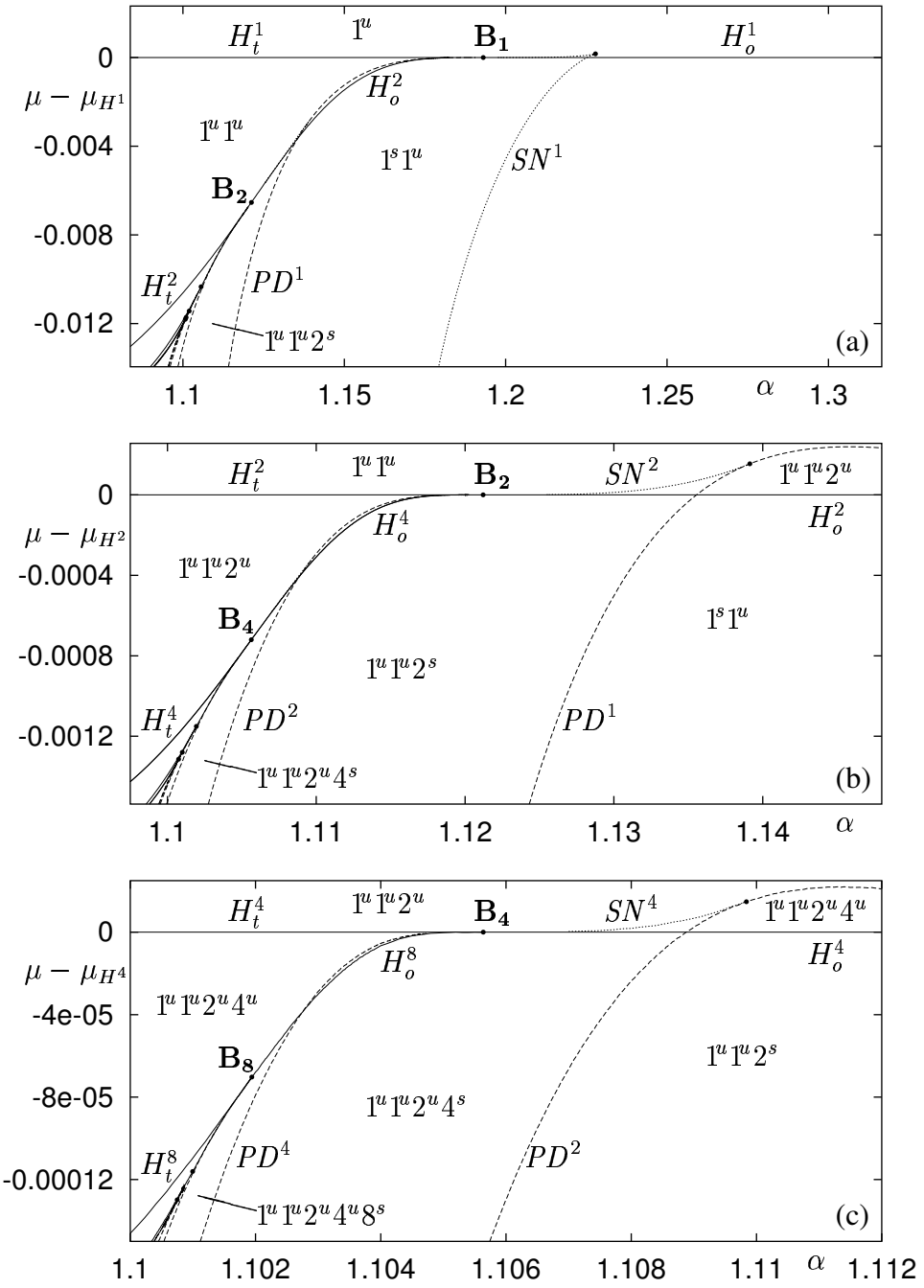


Fig. 8. The homoclinic-doubling cascade in Figure 7 drawn relative to the curve $H^1_{o/t}$ and two consecutive enlargements drawn relative to $H^2_{o/t}$ and $H^4_{o/t}$, respectively.

creasing $\tilde{\mu}$. The curve $PD^1$ was detected and this gave the opportunity to switch to the 2-periodic orbit $2^s$. This orbit was continued to the 2-homoclinic bifurcation curve $H_t^2$. The corresponding 2-homoclinic orbit then undergoes an inclination flip at $\mathbf{B_2}$. The results of the subsequent calculations follow exactly the same lines as those in section 3.3. Both homoclinic-doubling cascades follow a sequence of $\mathbf{B}$-

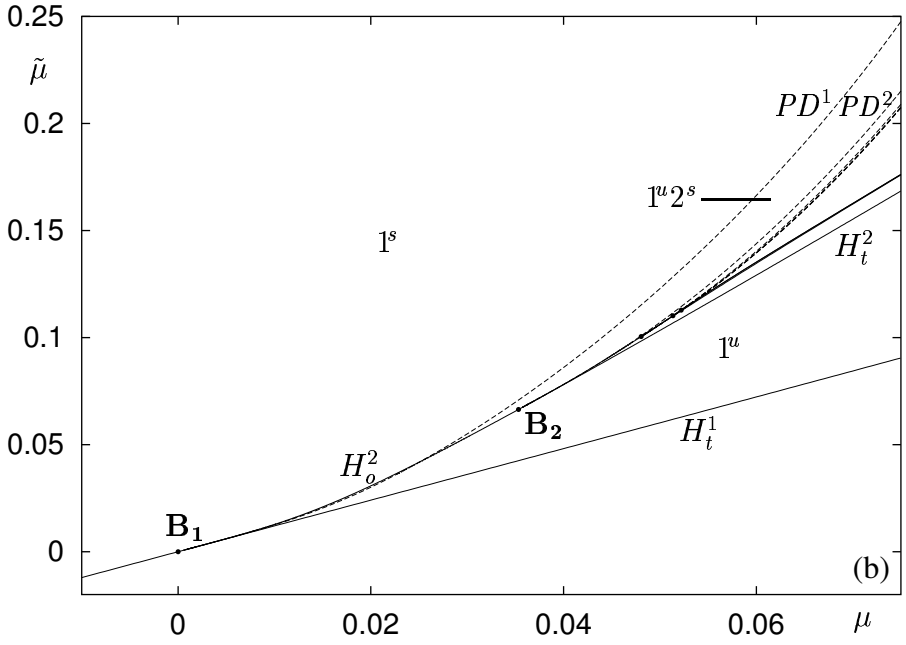


Fig. 9. A numerical picture of a homoclinic-doubling cascade in (1), where the primary homoclinic orbit undergoes an orbit flip at $\mathbf{B_1}$. All other $\mathbf{B}$-points are inclination flips. See the second row of Table 2 for the values of the other parameters.

type inclination flips after the initial homoclinic flip bifurcation $\mathbf{B_1}$.

Note the similarity with the inclination flip in Figure 7: a 180 degrees rotation of Figure 8 looks practically the same as the respective picture in Figure 10. Again, the self-similarity between succesive panels of Figure 10 is striking. This self-similarity is further investigated in the next section.

## 4 Scaling laws and renormalization

Figures 8 and 10 in the previous section show that the homoclinic-doubling cascade has a self-similar structure, and thus is governed by scaling laws. This behaviour was theoretically studied in [5] and [7]. In [5] a numerical investigation is performed of a piecewise-linear vector field, which is complemented and compared with results for an appropriate normal form, given by a one-dimensional unimodal map. The authors compare the scaling of the distances in parameter space between successive $\mathbf{B_n}$-points with the Feigenbaum constant of $4.6692\ldots$ [2]. In [7] a renormalization theory is given for a family of one-dimensional unimodal maps for $\lambda_s \geq 1/2$ and $\lambda_s - 1/2$ small (see Theorem 1), unfolding the equivalent of a homoclinic-doubling cascade. It turns out that there are two unstable eigenvalues of the renormalization operator. (All infinitely many other eigenvalues of the operator are strictly inside the unit disc.) These unstable eigenvalues are the

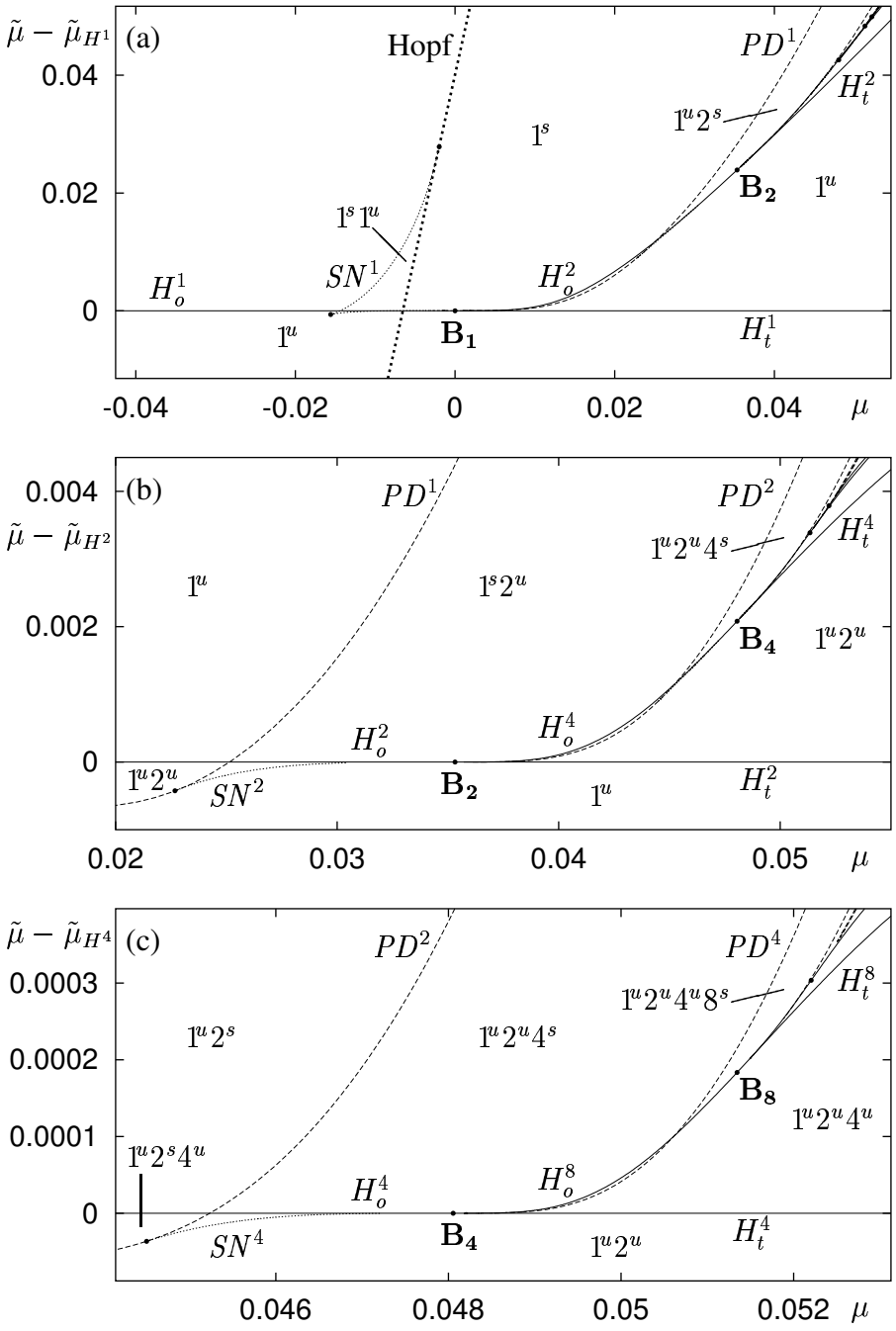


Fig. 10. The homoclinic-doubling cascade in Figure 9 drawn relative to the curve $H^1_{o/t}$ and two consecutive enlargements drawn relative to $H^2_{o/t}$ and $H^4_{o/t}$, respectively.

two scaling constants in the homoclinic-doubling cascade; see [7] for details. The first eigenvalue corresponds to the scaling of the "horizontal" distance between the points $\mathbf{B_n}$ and converges to 2 as $\lambda_s \to 1/2$ [5,7] and to the Feigenbaum constant 4.6692 as $\lambda_s \to 1$ [5]. The second eigenvalue governs the "vertical" contraction in the direction orthogonal to the homoclinic curves, as we explain later in this section. This constant goes to $\infty$ as $\lambda_s \to 1/2$ [7]. The two unstable directions of

the renormalization operator provide natural coordinates in which the renormalization is a simple affine map of the bifurcation diagram of the homoclinic-doubling cascade.

This paper is the first to investigate the homoclinic-doubling cascade for a smooth vector field and thus to confirm the existence of the two different scaling constants in practice. In this section the scaling constants are derived from our numerical computations and a comparison is made with the theoretical values which may be obtained from suitable one-dimensional maps.

To bring out these features and to facilitate the comparison with the results in [7], we chose coordinates in parameter space that are approximations of the natural coordinates of the renormalization analysis. This can be obtained by drawing the homoclinic-doubling cascade relative to a smooth curve, also called the envelope, that passes through all flip points $\mathbf{B_n}$ and is tangent to all bifurcation curves at these points. We approximated this envelope by cubic splines through the numerical data of the locations of the points $\mathbf{B_i}$. Bifurcation diagrams relative to this spline curve, together with one magnification for each, are shown in Figure 11 for the inclination flip and in Figure 12 for the orbit flip. The dotted horizontal axis in these figures corresponds to the spline we used. The respective boxes in panel (a) of Figures 11 and 12 are mapped by the renormalization operator onto the entire panel, as is clear from the enlargements in panel (b) of these figures. This emphasizes that the rescaling is an affine operation on in these coordinates. Two scaling factors are involved, a horizontal and vertical one, and they are easily read off the axes of the self-similar panels in these figures. The good agreement between the curves in panels (a) and (b) shows that the approximate splines we chose are indeed suitable.

The first three columns of Table 3 give an approximation to the horizontal scaling constant obtained from the data in Figure 11 for the cascade spawned from a primary inclination flip. To find this constant we considered the $\mathbf{B_n}$-points on the horizontal axis in Figure 11 and calculated $(\alpha_{i-1} - \alpha_{i-2})/(\alpha_i - \alpha_{i-1})$ for $i = 2, \ldots, 5$ where $\alpha_i$ is the $\alpha$ coordinate of $\mathbf{B_{2^i}}$. These values converge to a scaling constant of about $3.8$. This value is well between $2$ and $4.6692$. Since in this case $\lambda_s = 0.75$ this is what is expected. The first three columns of Table 4 present the same numerical data for the orbit flip case of Figure 12. For this case we were only able to calculate the homoclinic-doubling cascade up to $n = 16$. The resulting constant is again close to $3.8$. This is explained by the fact that both homoclinic-doubling cascades consist of inclination flips for $n \geq 2$.

The vertical contraction is the rate at which subsequent maxima of $H_o^{2^i}$ decrease in Figures 11 and 12. The maxima are collected in the first three columns of Tables 5 and 6. Although the two give similar results, it is difficult to give a prediction of the final contraction factor; an estimate is about $10$. This is due to the much stronger contraction and, therefore, lost numerical accuracy in the computations. In [7] this contraction was only predicted for eigenvalues $\lambda_s$ slightly larger than $1/2$, where

its rate goes to infinity as $\lambda_s \to 1/2$. However, through our numerical results, it can be seen that the strong contraction is clearly also present for $\lambda_s = 0.75$ and is indeed much stronger than the horizontal contraction in the sequence of successive $\mathbf{B_{2^i}}$-points.

To close this section, let us look more closely at a comparison between these numerically obtained scaling constants and those obtainable from the appropriate unimodal maps. In [5], a map governing a generic orbit flip is derived by looking at a Poincaré mapping on a plane transversal to the homoclinic orbit. This two-dimensional map can be further reduced to a one-dimensional map, essentially because of the existence of a homoclinic centre manifold [23,24]. The resulting "normal form map" is, for $\lambda_{ss}$ sufficiently large, given by the unimodal map [5]

$$f : \mathbb{R}_+ \to \mathbb{R}, \qquad x \mapsto (x - \frac{1+\lambda_s}{\lambda_s} r) x^{\lambda_s} + \frac{r^{1+\lambda_s}}{\lambda_s} + p. \tag{3}$$

Here $x$ represents, modulo a scaling, a coordinate on the intersection between a Poincaré section transversal to the homoclinic orbit and the center manifold $W^{s,u}$. The parameters $r$ and $p$ are such that $f'(r) = 0$ and $f(r) = p$. The envelope going through all the flip points corresponds to values of $(r, p)$ where the minimum of $f$ is equal to 0, hence $p = 0$ on this curve. Moreover, $r$ and $p$ are approximations of the natural coordinates of the renormalization operator mentioned before.

The interpretation of (3) is as follows. A homoclinic orbit corresponds to a periodic orbit of $f$ which goes through the point 0. If it additionally goes through the minimum of $f$, that is, a value of $(r, p)$ such that both $f^n(0) = 0$ and $f'(f^{n-1}(0)) = 0$, then this corresponds to an inclination flip $\mathbf{B_n}$. There exists a homoclinic-doubling cascade in the $(r, p)$-plane; see [5]. In particular, $(r, p) = (0, 0)$ corresponds to an orbit flip. Since $f$ is unimodal and thus has only one minimum, in this case $r = f^{n-1}(0)$ and $p = 0$. For the value $\lambda_s = 0.75$ which we used in our calculations in Section 3, we have calculated the sequence $r_i$ of $r$-values corresponding to $\mathbf{B_{2^i}}$ for $i = 0, \ldots, 5$. The results are in the last two columns of Table 4. Note that this sequence converges at a rate of 3.80, which complies with the rates calculated in [5]. The equation $f^n(0) = 0$ defines curves in the $(r, p)$-plane which correspond to all $H^i_{o/t}$ curves where $n$ is a multiple of $i$. The parameter $r$ is negative on these curves, so the minima of these curves correspond to maxima of the associated curves for the vector field. These minima were found graphically and are in the last two columns of Table 6. The respective scaling constant converges to 11.6. All numerical data obtained from the map corresponds nicely with the numerical data in the vector fields in the second and third column of Tables 4 and 6.

For the cascade spawned from an inclination flip a different map must be used for modelling the initial homoclinic flip bifurcation. We derived this map in the same

way as (3) was derived in [5] and it is, again for $\lambda_{ss}$ large enough, given by

$$g : \mathbb{R}_+ \to \mathbb{R}, \qquad x \mapsto p + r^{2\lambda_s} - 2(rx)^{\lambda_s} + x^{2\lambda_s}. \tag{4}$$

The parameters $r$ and $p$ have the same properties and interpretation as before, but here $(r, p) = (0, 0)$ corresponds to the primary inclination flip. The results of a numerical analysis of this map are in the last two columns of Tables 3 and 5. They reveal a scaling constant of $3.80$ for the sequence $r_i$ of $r$-values and of $11.5$ for the minima of $p$. Both scaling constants agree nicely with the data obtained from the vector fields in the second and third column of Tables 3 and 5.

In summary, we have found the scaling constants for a smooth vector field and they are in good agreement with the theory for one-dimensional maps. Notice that the scaling constants of both $f$ and $g$, that is, both the cascades where the primary homoclinic bifurcation is an orbit flip and where it is an orbit flip, are the same as $n \to \infty$. This is what we expected, because both cascades consist of a sequence of inclination flips.

| | Vector field (1) | | Unimodal map $g$ in (4) | |
|---|---|---|---|---|
| Point | Position $\alpha_i$ | $\frac{\alpha_{i-1} - \alpha_{i-2}}{\alpha_i - \alpha_{i-1}}$ | Position $r_i$ | $\frac{r_{i-1} - r_{i-2}}{r_i - r_{i-1}}$ |
| $\mathbf{B_1}$ | 1.193035 | | 0 | |
| $\mathbf{B_2}$ | 1.121214 | | 1 | |
| $\mathbf{B_4}$ | 1.105637 | 4.6107 | 1.685874 | 1.45799 |
| $\mathbf{B_8}$ | 1.101941 | 4.215 | 1.909693 | 3.06441 |
| $\mathbf{B_{16}}$ | 1.100995 | 3.91 | 1.971955 | 3.5948 |
| $\mathbf{B_{32}}$ | 1.100750 | 3.86 | 1.988577 | 3.7458 |
| Limit | 1.100663 | 3.80 | 1.9945 | 3.80 |

Table 3
Scaling constant (accumulation rate) for the homoclinic-doubling cascade spawned from a primary *inclination flip* for the eigenvalues used in this paper for (1) (second and third column) and the map $g$ in (4) (right two columns). The values $\alpha_i$ and $r_i$ are the $\alpha$- and $r$-coordinates of the respective points $\mathbf{B_i}$. The limits are approximate extrapolations. Notice the good agreement of the scaling constants.

## 5 Conclusions

The numerical investigations in this paper confirm the theory of [6,19] and supplement the numerical investigations in [5] about the existence of a homoclinic-doubling cascade. Here, for the first time the cascade has been shown to exist in a smooth vector field. We considered the two different cases where the primary homoclinic orbit undergoes an inclination flip and where it undergoes an orbit flip. As

| | Vector field (1) | | Unimodal map $f$ in (3) | |
|---|---|---|---|---|
| Point | Position: $\mu_i$ | $\frac{\mu_{i-1}-\mu_{i-2}}{\mu_i-\mu_{i-1}}$ | Position: $r_i$ | $\frac{r_{i-1}-r_{i-2}}{r_i-r_{i-1}}$ |
| $\mathbf{B_1}$ | 0 | | 0 | |
| $\mathbf{B_2}$ | $3.532379 \cdot 10^{-2}$ | | 0.6814202 | |
| $\mathbf{B_4}$ | $4.805438 \cdot 10^{-2}$ | 2.774717 | 0.9540395 | 2.499530 |
| $\mathbf{B_8}$ | $5.134454 \cdot 10^{-2}$ | 3.86929 | 1.0306196 | 3.55992 |
| $\mathbf{B_{16}}$ | $5.220320 \cdot 10^{-2}$ | 3.8322 | 1.0511243 | 3.73476 |
| Limit | $5.25 \cdot 10^{-2}$ | 3.80 | 1.05848 | 3.801 |

Table 4
Scaling constant (accumulation rate) presented as in Table 3 for the homoclinic-doubling cascade spawned from a primary *orbit flip*.

| | Vector field (1) | | Unimodal map $g$ in (4) | |
|---|---|---|---|---|
| Curve | Maximum: $\mu_i$ | Factor: $\frac{\mu_{i-1}}{\mu_i}$ | Minimum: $p_i$ | Factor: $\frac{p_{i-1}}{p_i}$ |
| $H_o^2$ | $6.282 \cdot 10^{-4}$ | | $-3.70370 \cdot 10^{-2}$ | |
| $H_o^4$ | $6.617 \cdot 10^{-5}$ | 9.494 | $-4.93295 \cdot 10^{-3}$ | 7.50808 |
| $H_o^8$ | $5.340 \cdot 10^{-6}$ | 12.39 | $-4.77748 \cdot 10^{-4}$ | 10.3254 |
| $H_o^{16}$ | | | $-4.27892 \cdot 10^{-5}$ | 11.1652 |
| Limit | | | | 11.5 |

Table 5
Vertical scaling constant (contraction rate) for the homoclinic-doubling cascade spawned from a primary *inclination flip* for the eigenvalues used in this paper for (1) (second and third column) and the map $g$ in (4) (right two columns). The maxima $\mu_i$ for the vector field are with respect to a suitable spline and the minima $p_i$ for the one-dimensional map are with respect to to the $r$ axis. The limit is an approximate extrapolation. Note the similarity between the third and the fifth column.

predicted by the theory, the two cases are similar, both in behaviour and in the shape of the bifurcation diagrams, because all homoclinic flip bifurcations except (possibly) the first one are inclination flips. Figures 7 and 9 clearly show how both kinds of homoclinic-doubling cascades cause the death of a period-doubling cascade.

As already mentioned in Section 2, the homoclinic-doubling cascades investigated in this paper arise in the unfoldings of codimension-three resonant homoclinic flip bifurcations in which the eigenvalues are on the border between the $\mathbf{B}$ and $\mathbf{C}$ type homoclinic flips; see [19]. To study these unfoldings, one can perform numerical investigations on a sphere around this codimension-three point in parameter space. This will be addressed in our forthcoming paper [29].

Using AUTO/HOMCONT it is relatively straightforward to find a codimension-

| | Vector field (1) | | Unimodal map $f$ in (3) | |
|---|---|---|---|---|
| Curve | Maximum: $\tilde{\mu}_i$ | Factor: $\frac{\tilde{\mu}_{i-1}}{\tilde{\mu}_i}$ | Minimum: $p_i$ | Factor: $\frac{p_{i-1}}{p_i}$ |
| $H_o^2$ | $-1.820 \cdot 10^{-3}$ | | $-4.82204 \cdot 10^{-2}$ | |
| $H_o^4$ | $-1.996 \cdot 10^{-4}$ | 9.118 | $-3.58164 \cdot 10^{-3}$ | 13.4632 |
| $H_o^8$ | $-1.546 \cdot 10^{-5}$ | 12.91 | $-2.94591 \cdot 10^{-4}$ | 12.1580 |
| $H_o^{16}$ | | | $-2.52439 \cdot 10^{-5}$ | 11.6698 |
| Limit | | | | 11.4 |

Table 6
Vertical scaling constant (contraction rate) presented as in Table 5 for the homoclinic-doubling cascade spawned from a primary *orbit flip*.

three resonant homoclinic flip bifurcation numerically. However, as we have shown, finding actual homoclinic-doubling cascades involves many more steps. In Section 3.2 we gave a general algorithm to find such cascades and similar bifurcation structures. While this is a systematic approach, the switching between $n$-homoclinic and $2n$-homoclinic orbits involves several indirect steps. Namely, switching from a homoclinic orbit to its bifurcating periodic orbit, which after period-doubling is continued back to a homoclinic-doubled orbit. Another algorithmic strategy, *direct* branch-switching at a $\mathbf{B}$- or $\mathbf{C}$-type homoclinic flip point from an $n$- to a $2n$-homoclinic orbit, would be desirable. However, this idea is not as straightforward as it might sound, owing to the exponential closeness of the two bifurcation curves in parameter space. Furthermore, the $2n$-homoclinic orbit in phase space is very close to two copies of the original $n$-homoclinic orbit. These issues will be addressed in future work.

The theory [6,19] predicts that, in addition to a sequence of period-doublings, saddle-node bifurcations of limit cycles and $2^m$-homoclinic orbits for arbitrary $m$, there must be a region with horseshoe dynamics (chaos). It is present in the region in the lower left hand side corner of Figure 7 and in the top right corner of Figure 9, past the homoclinic-doubling cascade. Also present are so called "bubbles" consisting of homoclinic-doubling cascades where the primary orbit is an $n$-homoclinic orbit for arbitrary $n > 1$. This was not investigated in this paper, since we have concentrated only on the bifurcation curves of the homoclinic-doubling cascade itself. It would be an interesting topic for future research to compare the strange attractors inherent in the accumulation of period-doubling cascades with those predicted by the homoclinic-doubling cascade normal forms given by one-dimensional maps.

It should be stressed that Sandstede's model (1) was specifically *constructed* to contain inclination flips and orbit flips and is not, as far as we know, a model for any physical process. However, there are applications in which inclination flips occur, for example, the ones mentioned in the introduction. Homoclinic-doubling cascades are expected to occur in these applications, and this will also be addressed in

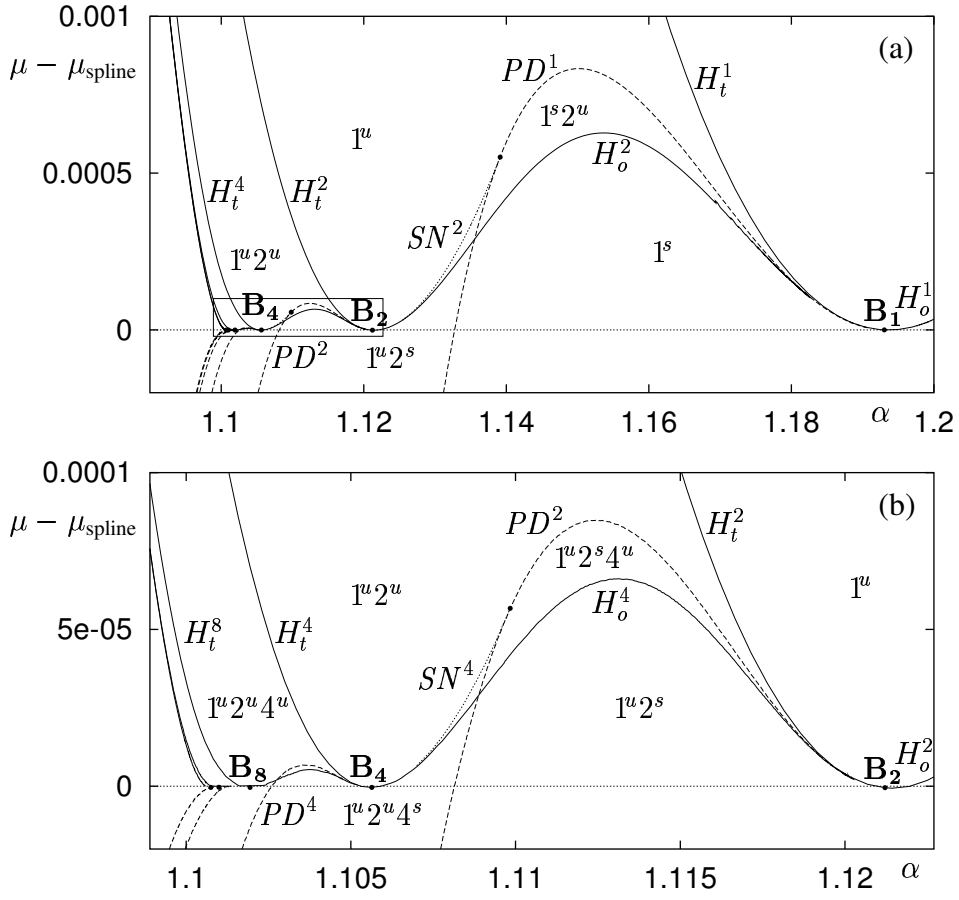


Fig. 11. The homoclinic-doubling cascade in Figure 7 drawn relative to a spline through all the $\mathbf{B}$-points, that is, in an approximation of the natural coordinates of the renormalization operator. The box in panel (a), enlarged in panel (b), is taken to panel (a) by simple rescaling of the horizontal and vertical axes. The respective scaling constants can be read off the axis and are summarized in Tables 3 and 5.

future work. More generally, our motivation in studying Sandstede's model was to demonstrate an algorithmic approach for finding homoclinic-doubling cascades numerically. The homoclinic-doubling cascade is a generic mechanism for the death of a period-doubling cascade and as such should be found in many physical systems. Indeed, the ubiquity of period-doubling cascades is famous! We hope, therefore, to have provided the reader with a framework and numerical procedures to find homoclinic-doubling cascades for themselves in models from many different areas of applied science.

## References

[1] P. Cvitanovic. *Universality in Chaos*. Adam Hilger, 2nd edition, 1989.

[2] M. Feigenbaum. Quantitative universitality for a class of nonlinear transformations.

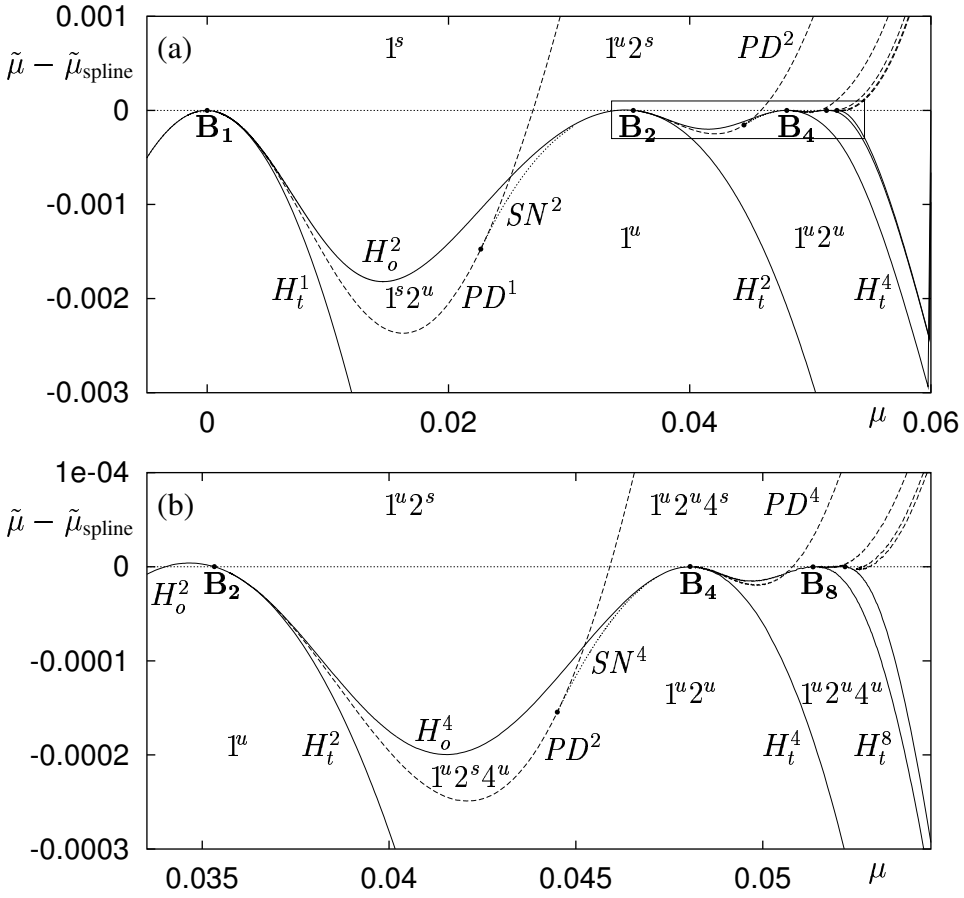


Fig. 12. The homoclinic-doubling cascade in Figure 9 drawn drawn similarly to Figure 11. The box in panel (a), enlarged in panel (b), is taken to panel (a) by simple rescaling of the horizontal and vertical axes. The respective scaling constants can be read off the axis and are summarized in Tables 4 and 6.

*J. Stat. Phys*, 19:25–52, 1978.

[3] E. Knobloch, D. R. Moore, J. Toomre, and N. O. Weiss. Transitions to chaos in two-dimensional double-diffuse convection. *Journal of Fluid Mechanics*, 166:409–448, 1986.

[4] S. M. Wieczorek, B. Krauskopf, and D. Lenstra. A unifying view of bifurcations in a semiconductor laser subject to optical injection. *Optics Communications*, 172(1-6):279–295, 1999.

[5] H. Kokubu, M. Komuru, and H. Oka. Multiple homoclinic bifurcations form orbit-flip. i. successive homoclinic doublings. *International Journal of Bifurcation and Chaos*, 6(5):833–850, 1996.

[6] A. J. Homburg, H. Kokubu, and V. Naudot. Homoclinic doubling cascades. DANSE preprint, `http://www.math.fu-berlin.de/~Dynamik/preprints/homburg_97_homdoubling.ps.gz`, 1997.

[7] A. J. Homburg and T. Young. Universal scalings in homoclinic doubling

cascades. DANSE preprint, http://www.math.fu-berlin.de/~Dynamik/preprints/homburg_99_renormalization.ps.gz, 1999.

[8] J. Guckenheimer and P. Holmes. *Nonlinear Oscillations, Dynamical Systems and Bifurcations of Vector Fields*. Springer, 1983.

[9] B. Sandstede. *Verzweigungstheorie homokliner Verdopplungen*. PhD thesis, Freie Universität Berlin, Institut für Angewandte Analysis und Stochastic, 1993. Report No. 7, Berlin.

[10] M. Kisaka, H. Kokubu, and H. Oka. Bifurcations to $N$-homoclinic orbits and $N$-periodic orbits in vector fields. *Journal of Dynamics and Differential Equations*, 5:305–357, 1993.

[11] M. Kisaka, H. Kokubu, and H. Oka. Supplement to homoclinic-doubling bifurcation in vector fields. In R. Bamon, R. Labarca, J. Lewowicz, and J. Palis, editors, *Dynamical Systems*, pages 92–116. Longman, 1993.

[12] V. Naudot. *Bifurcations Homoclines des Champes de Vecteurs en Dimension Trois*. PhD thesis, l'Université de Bourgogne, Dijon, 1996.

[13] M. Krupa, B. Sandstede, and P. Szmolyan. Fast and slow waves in the FitzHugh-Nagumo equation. *Journal of Differential Equations*, 133:49–97, 1997.

[14] M. Koper. Bifurcations of mixed-mode oscillations in a three-variable autonomous Van der Pol-Duffing model with a cross shaped phase diagram. *Physica D*, 80:72–94, 1995.

[15] A. R. Champneys and Yu. A. Kuznetsov. Numerical detection and continuation of codimension-two homoclinic bifurcations. *International Journal of Bifurcation and Chaos*, 4(4):785–822, 1994.

[16] A. Shil'nikov. On bifurcations of the Lorenz attractor in the Shimizu-Morioka model. *Physica D*, 62:338–346, 1993.

[17] A. M. Rucklidge. Chaos in a low-order model of magnetoconvection. *Physica D*, 62:323–337, 1993.

[18] P. Gaspard, A. Arnéodo, R. Kapral, and C. Sparrow, editors. *Homoclinic chaos*, Physica D 62 (Special Issue), 1993.

[19] A. J. Homburg and B. Krauskopf. Resonant homoclinic flip bifurcations. DANSE preprint 53/98, http://www.math.fu-berlin.de/~Dynamik/preprints/homburg_98_homcod3.ps.gz, 1998.

[20] B. Sandstede. Constructing dynamical systems having homoclinic bifurcation points of codimension two. *Journal of Dynamics and Differential Equations*, 9(2):269–288, 1997.

[21] A. R. Champneys, Yu. A. Kuznetsov, and B. Sandstede. A numerical toolbox for homoclinic bifurcation analysis. *International Journal of Bifurcation and Chaos*, 6(5):867–887, 1996.

[22] E. J. Doedel, A. R. Champneys, T. F. Fairgrieve, Yu. A. Kuznetsov, B. Sandstede, and X. Wang. AUTO 97: Continuation and bifurcation software for ordinary differential equations (with HomCont), `http://indy.cs.concordia.ca/auto`, 1997.

[23] B. Sandstede. Center manifolds for homoclinic solutions. Accepted by Journal of Dynamics and Differential Equations, `http://www.math.ohio-stae.edu/~sandsted/Paper/center.ps.gz`, 1999.

[24] M. V. Shashkov and D. V. Turaev. An existence theorem of smooth nonlocal center manifolds for systems close to a system with a homoclinic loop. *J. Nonlinear Sci.*, 9:525–573, 1999.

[25] L. Shil'nikov. On a new type of bifurcation of multidimensional dynamical systems. *Sov. Math. Dokl.*, 10:1368–1371, 1969.

[26] B. Deng. The Shil'nikov problem, exponential expansion, strong $\lambda$-lemma, $C^1$-linearization, and homoclinic bifurcation. *Journal of Differential Equations*, 79:189–231, 1989.

[27] S. N. Chow, B. Deng, and B. Fiedler. Homoclinic bifurcation at resonant eigenvalues. *Journal of Dynamics and Differential Equations*, 2(2):177–244, 1990.

[28] S. Nii. $N$-homoclinic bifurcations for homoclinic orbits changing their twisting. *Journal of Dynamics and Differential Equations*, 8:549–572, 1996.

[29] B. E. Oldeman, B. Krauskopf, and A. R. Champneys. Numerical investigation of resonant homoclinic flip bifurcations I: The single homoclinic-doubling case. Preprint, to be finished, `http://www.fen.bris.ac.uk/engmaths/research/reports/99r10.ps.gz`, 1999.